EFFICIENT UTILIZATION OF Al_2O_3 AS STRUCTURAL PROMOTER OF Fe INTO 2 AND 3 STEPS CHEMICAL LOOPING HYDROGEN PROCESS: PURE H_2 PRODUCTION FROM ETHANOL

Martina Damizia [a], Maria P. Bracciale [a,], Francesco Anania [a], Lingyu Tai [b], Paolo De Filippis [a], Benedetta de Caprariis [a]*

[a] Department of Chemical Engineering Materials Environment, SAPIENZA University of Rome, Via Eudossiana 18, 00184, Rome (Italy)

[b] Key Laboratory of Agro-Forestry Environmental Processes and Ecological Regulation of Hainan Province-College of Ecology & Environment, Hainan University, 570228, Haikou (China)

* Corresponding Author: mariapaola.bracciale@uniroma1.it

ABSTRACT

Chemical Looping Hydrogen (CLH) allows the direct production of pure hydrogen exploiting the redox properties of Fe, with high flexibility on the type of reductant used. In this work, a highly pure hydrogen stream suitable for the direct use into Proton Exchange membrane Fuel Cells was produced, using bioethanol as renewable fuel. The influence of both redox temperature (675°C-750°C) and chemical composition of the Fe-based particles (2 wt% and 40 wt% of alumina added) on the carbon formation rate during reduction step was also deeply analyzed. Al_2O_3 changed both Fe_xO_y redox kinetics and equilibrium phases, leading to a complete iron deactivation at high Al_2O_3 concentration. The addition of an air oxidation step (3 steps CLH) is fundamental to restore the redox activity, with a constant efficiency of about 30 % at 750 °C for 10 cycles. Furthermore, Al_2O_3 promotes the ethanol conversion into carbon, undermining the hydrogen purity.

KEYWORDS: Hydrogen, Chemical looping, Al_2O_3, Water Splitting, Iron Oxide

INTRODUCTION

The development of Proton Exchange membrane fuel cells (PEMFCs) allows the use of H_2 as alternative clean fuel especially in the automotive sector [1]. To avoid the deactivation of the Pt-based catalyst of the cells, pure H_2 streams with a maximum CO concentration of 10 ppm is required [2]. In the traditional steam methane reforming plant[3,4] [5], the H_2 purity target is reached by adding several separation units to the reformer, with a consequent increase of H_2 final cost [6]. Furthermore, the study and the optimization of H_2 extraction process from renewable

sources (water and biomass) are fundamental to supply clean, affordable, and secure energy from H_2 and to reach the goal of carbon neutrality in 2050 [7].

Chemical looping hydrogen processes (CLH) allow the direct production of pure and renewable H_2, exploiting the redox properties of the transition metals [8]. Iron is one the most studied element due to its low cost, its wide availability and the favorable thermodynamics when used in looping reactions [9,10]. In the presence of Fe, the process can involve different configurations based on 2 or 3 spatially and temporary separated phases [11]. In the 2 steps CLH, hematite (Fe_2O_3) is first reduced using a fuel to metallic iron. The metal reduction is reached at the expense of the fuel oxidation by the lattice oxygen atoms of the metal oxide, producing mainly CO_2 and H_2O as gaseous by-products. Then, in the steam oxidation step, Fe is oxidized producing pure H_2 and restoring the metal oxide (magnetite, Fe_3O_4), which can participate in a subsequent redox cycle [12]. At the end of the steam oxidation, Fe_2O_3 cannot be restored due to thermodynamics limitations occurring using steam as oxidant [13]. An air oxidation step must be added after the steam oxidation (3 step CLH) to re-establish Fe_2O_3 at the end of each cycle [14,15]. If a renewable fuel is used in the reduction step, pure H_2 is also obtained in a completely green way. The use of renewable reductants to produce green H_2 has been already investigated by several authors. Xu et al. [16] studied the feasibility to produce H_2 from biomass pyrolysis gas in a fluidized bed reactor using modified iron ores as redox material. The results showed that the NiO–iron ore was the best material for hydrogen production leading to the highest hydrogen yields and purity (8.89 mmol/g and 99.02 %) with high cycle performance (10 consecutive cycles). Situmorang et al. [17] report a novel H_2 production scheme based on the conversion of biomass into H_2 by pyrolysis. H_2 is produced from bio-oil steam reforming and by chemical looping technology using the biochar as renewable reducing agent of Fe_3O_4. Under the optimum condition, about 6.9 kg/h of hydrogen

could be produced from 100 kg/h of wood biomass. Kong et al. [18] present a simulation study of a Fe-based chemical looping process to convert biogas into H_2. The results are compared with a traditional steam methane reforming plant. The data confirm the great potential of applying CLH technology for a future carbon negative economy.

The main drawbacks of the 2 steps CLH configuration are the low thermal stability of iron oxides at repeated cycles and the carbon deposition during the reduction step caused by the utilization of a carbonaceous fuel. At the operative conditions required for iron oxides reduction, the thermal cracking of the carbonaceous reductant is favored, resulting in the formation of solid carbon, which undermines both the hydrogen purity and the particle reactivity. If the carbon deposition occurs, in fact, carbon can react with water during the steam oxidation step producing CO by gasification, a poison of the fuel cell catalyst [19]. Furthermore, a fraction of solid carbon can remain on the particle's surface after the water oxidation step and can block the Fe active sites, contributing to their deactivation at high number of redox cycles [20,21].

In authors' previous work, pure H_2 by 2 steps CLH is obtained using bioethanol as reducing agent and pure Fe_2O_3 as redox material. A relationship between the amount of ethanol fed in the reduction and the purity of H_2 was demonstrated [22,23]. Specifically, if the complete reduction to Fe is avoided by monitoring the amount of ethanol fed, the lattice oxygen atoms of iron oxide are still able to convert solid carbon into CO and CO_2, preventing its deposition and therefore guarantying a pure H_2 stream in oxidation.

One of the major issues to be solved is the low thermal stability of iron oxides causing the decay of iron reactivity at consecutive redox cycles due to sintering phenomena. Many works in literature studied the effect of adding high thermal stability material to iron oxides on particle performances. Different materials have been tested as structural promoters including Al_2O_3, MgO, ZrO_2, TiO_2

with promising results in terms of particle thermal resistance [24–26]. However, structural promoter affects the particle morphology and the redox reactions pathway of iron, in different extents depending on the particle synthesis method, the amount of promoter added and the operative conditions chosen [25].

Al_2O_3 is one of the most studied materials, widely used as a catalytic support into many chemical reactions [27]. Its utilization into chemical looping process still requires a deep investigation due to its active role in the process when iron is used as redox element [28]. Al_2O_3 in fact can interact with iron forming a spinel structure named hercynite ($FeAl_2O_4$) which totally changes the particle reactivity in looping reactions [25]. Based on literature data, the $FeAl_2O_4$ results from the reaction between wüstite (FeO) and Al_2O_3 according to reaction 1 [29,30].

$$FeO + Al_2O_3 \leftrightarrow FeAl_2O_4 \qquad (1)$$

Furthermore, due to its acidic nature, Al_2O_3 catalyzes cracking reactions in the presence of a carbonaceous reducing agent, enhancing the carbon formation during the reduction step and therefore the hydrogen purity [31,32].

The goal of this article is to make possible the use of bioethanol as carbonaceous reductant of iron oxide to produce pure hydrogen, suitable for direct use in PEMFC by CLH process. Bioethanol is a non-toxic and stable liquid specie at ambient condition and so its distribution and utilization as feedstock for CLH process, especially in-situ H_2 production for automotive sector, can considerably enhance the whole process efficiency by lowering the security issues related to the storage, transportation, and use of gaseous reductant (CO, syngas, biogas). However, the use of bioethanol in this process is not trivial, its high C/H ratio promotes carbon deposition hindering the hydrogen purity. Studies on the use of bioethanol as renewable fuel in chemical looping processes are mainly focused on the production of syngas (chemical looping reforming, CLR),

were the lattice oxygen of the metal oxide was exploited to supply pure O_2 needed to the bioethanol partial oxidation to syngas. The subsequent oxidation step was performed with air as oxidizer. Only few works in literature reports the production of hydrogen by CLH processes with bioethanol as reductant and in any case the purity of the obtained hydrogen stream is not suitable for the direct use in PEMFC (Table 1). Therefore, the use of bioethanol in CLH processes aimed at the direct production of pure H_2 still need to be optimized.

Table 1. Main results of published works on chemical looping processes with bioethanol as renewable fuel (CLR: chemical looping reforming; CLH: Chemical Looping Hydrogen).

	Reducer	**Oxidizer**	**Sample**	**Target product**	**H_2 purity**	**Ref.**
CLR	bioethanol	air	Ni/Mn_2O_4	syngas	68 %	[33]
CLR	bioethanol	air	Ni/CeO_2	syngas	80 %	[34]
CLR	bioethanol	air	Ni	syngas	61.5 %	[35]
CLH	bioethanol	steam	Fe/Mn	H_2	70 %	[36]
CLH	bioethanol	steam	Ni/Fe_2O_3	H_2	85 %	[37]
CLH (this work)	bioethanol	steam	Fe_2O_3/Al_2O_3	H_2	100 %	

Taking these aspects into account, in this work a pure H_2 stream is produced by using Fe_2O_3-Al_2O_3 particles as redox material and bioethanol as reductant. The interaction between Fe and Al is deeply studied in the 2 steps CLH configuration. To better understand the effect of Al_2O_3 addition on particle's performance, two different amounts of alumina are added to iron oxide (2 wt% and 40 wt% of the total mass). Samples are synthetized by coprecipitation method and tested at two different temperatures (675 °C and 750 °C) for 10 redox cycles to find the optimal conditions which maximize the H_2 yields and purity. The influence of the variation of temperature on ethanol decomposition products is also studied. For comparison purposes, experiments are also conducted on pure Fe_2O_3 synthetized by the same method. The sample with 40 wt% Al content is also tested into a 3 steps CLH (reduction-steam oxidation-air oxidation) configuration.

EXPERIMENTAL SECTION

Materials for Fe-based particles synthesis. Fe-based particles were synthesized starting from metal nitrate salts used as received (Iron nitrate nonahydrate ($Fe(NO_3)_3 \cdot 9H_2O$), Aluminium nitrate nonahydrate ($Al(NO_3)_3 \cdot 9H_2O$). 30 wt% ammonia solution (NH_4OH) was used as precipitation agent.

Fe-based particles synthesis and bench scale plant details. The Fe-based particles were synthesized by coprecipitation method from the nitrate metal salts following the procedure explained in details in the author's previous work [38]. After the synthesis, the particles were first dried in an oven heated at 110 °C for 24 h and then calcined with air in a muffle furnace at 350 °C for 2 h and 900 °C for 2 h. The obtained samples were grounded and sieved in the range of size 125 μm-20 μm. The resulting samples were named 100Fe, for pure Fe_2O_3; 98Fe2Al, for 98 wt% Fe_2O_3-2 wt% Al_2O_3; 60Fe40Al for 60 wt% Fe_2O_3-40 wt% Al_2O_3. The particle's activity was tested in a fixed bed reactor at two different reaction temperatures (675 °C and 750 °C) maintaining the pressure constant at 1 bar. The fixed bed was constituted by 1 gram of Fe-based particles. The bench scale plant is described in details in the author's previous works [22,38].

The 2 steps CLH tests were conducted feeding alternatively ethanol in the reduction step and water in oxidation with a constant flowrate of 4 mL/h, in the presence of Argon as carrier gas (250 mL/min). In the 3 steps CLH experiments air was also fed to the reactor with a constant flowrate of 500 mL/min.

Ethanol decomposition tests (blank tests) were conducted loading the reactor with 1 gram of SiO_2 and by feeding ethanol for 30 minutes, keeping constant the flowrate to 4 mL/h.

Fe-based particles Characterization. The Fe-based particles before and after the stability tests were characterized by X-ray powder diffraction (XRD). XRD patterns were acquired using a

Philips Analytical PW1830 X-ray diffractometer, equipped with a Ni β-filtered Cu Kα (1.5418 Å) radiation, in the 2θ range from 15 to 80° with a step size of 0.02° and a time for step of 2 s. The data were collected with an acceleration voltage and applied current of 40 kV and 30 mA, respectively. The crystalline phases in the resulting diffractograms were identified through the COD database (Crystallography Open Database – an open access collection of crystal structures) [39]. Surface area was determined by N_2 adsorption-desorption isotherms acquired at -196 °C using a Micromeritics Triflex analyzer (Micromeritics Instrument Corp.). The adsorption-desorption isotherms were acquired in the p/p^0 range from 0.01 to 0.99. Isotherm analysis was performed using the 3Flex Version 4.05 software. Samples were previously outgassed at 300 °C for 4 h. The BET equation was used to determine the specific surface area.

The oxygen transport capacity of the samples was measured by temperature-programmed reduction (TPR) experiments with a thermogravimetric analyzer SDTQ600 (TA Instruments). The samples were pre-treated under argon flow at 100 °C for 10 min to remove adsorbed moisture and air. Then the TPR profiles were recorded by heating the sample from 100 °C to 1000 °C at 10 °C/min under a H_2 flow (5 % H_2 in Ar, 100 mL/min). The deconvolution of the TPR profiles is also performed to identify the effect of the Al_2O_3 in the mechanism and kinetics of reduction of iron oxides. In fact, deconvolution allows to break down every single sample's reduction step, providing useful information to deepen the properties of the material. The deconvolution of TPR curves was performed according to the Gaussian–Lorentzian Cross Product expression as a fitting function using PeakFit software.

RESULTS AND DISCUSSION

Fe-based particles Characterization. XRD analysis were performed on the samples 60Fe40Al and 98Fe2Al before and after the stability test (10 consecutive redox cycles) at 675 °C and 750 °C

in the 2 step CLH configuration (reduction-steam oxidation). The stability test ends with the steam oxidation of the samples. The obtained diffractograms are reported in Figure 1. The pattern of the sample 98Fe2Al after the stability test at 750 °C overlaps with that at 675 °C and therefore it is not reported.

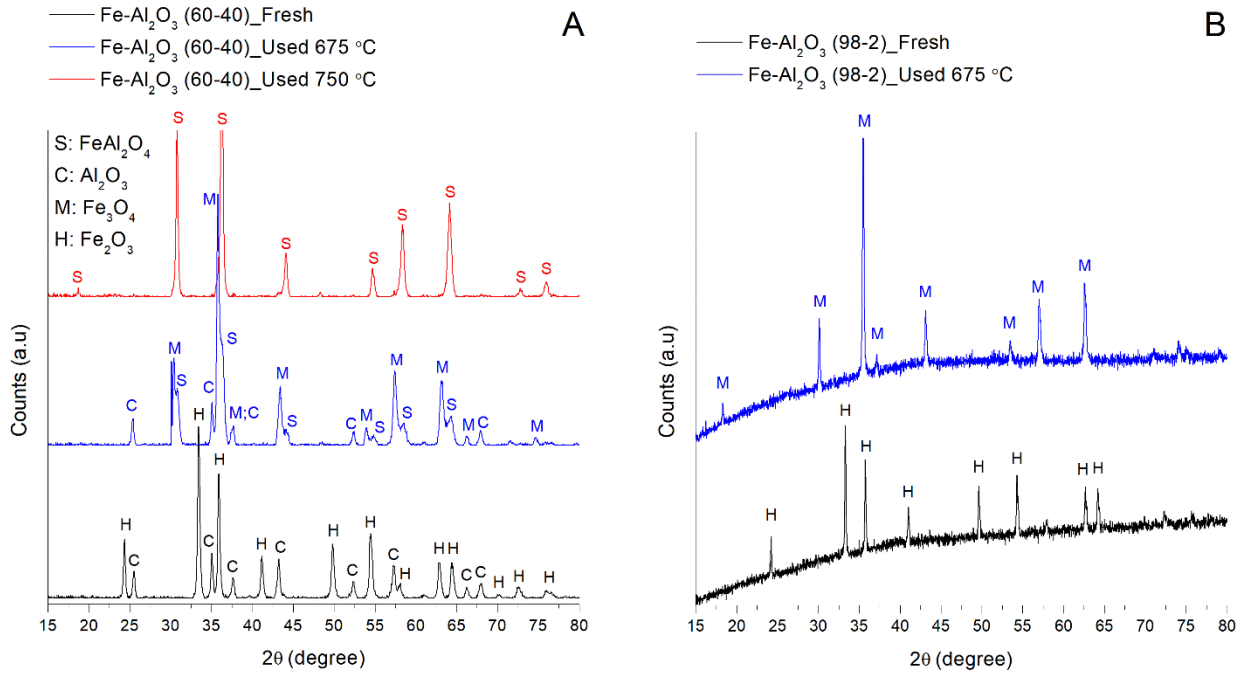

Figure 1. XRD patterns of the sample 60Fe40Al (A) and 98Fe2Al (B) before and after the stability tests at 675 °C and 750 °C. (H: Fe_2O_3, M: Fe_3O_4, C: Al_2O_3, S: $FeAl_2O_4$).

The pattern of the fresh sample 98Fe2Al shows only the peaks related to Fe_2O_3 suggesting that the amount of free crystalline alumina in the sample is lower than the detection limit of the XRD technique used [40,41]. The same results are obtained for the sample 98Fe2Al after the stability tests in all the range of temperature studied, no signals for Al_2O_3 are detected and iron is present only in the crystal phase of magnetite (Fe_3O_4). At the end of the stability test in fact, Fe_2O_3 cannot be restored by steam oxidation and only magnetite is formed due to thermodynamics limitations. Furthermore, no $FeAl_2O_4$ phase is detected in any process step; if a chemical interaction between

Fe and Al occurs, it regards only a small amount of the sample and it is lower than the detection limit of XRD analysis.

A particular behavior is detected for the sample 60Fe40Al. Unlike 98Fe2Al, the XRD pattern of the fresh 60Fe40Al shows the signals related to the two separated oxides (Fe_2O_3 and Al_2O_3). Furthermore, looking at the 60Fe40Al pattern after stability tests, the crystal phases detected change and the influence of reaction temperature on the interaction between Fe and Al is clearly visible. At 675 °C the crystal phases are magnetite (Fe_3O_4), hercynite ($FeAl_2O_4$) and corundum (Al_2O_3) while by increasing the reaction temperature until 750 °C, the signals of free Al_2O_3 at the end of the test disappears, and only the peaks for $FeAl_2O_4$ are detected.

The sample surface area is a key parameter of the process since it directly affects the sample reactivity. To evaluate the structural modification during the consecutive redox cycles, BET analysis are conducted on the samples before and after the stability tests at all the tested temperatures. For comparison purpose, BET analysis is also conducted on the sample 100Fe before and after tests. The BET surface area values are summarized in Table 2.

Table 2. BET values (m^2/g) of the samples before and after the stability tests as a function of temperature.

	Fresh sample	**675 °C**	**750 °C**
100Fe			
2 steps	0.7	0.6	0.2
98Fe2Al			
2 steps	1.2	1.1	1.0
60Fe40Al			
2 steps	9.0	1.3	1.2
3 steps	9.0	6.2	6.2

The fresh sample 100Fe owns the lowest surface area equal to 0.7 m^2/g, which after stability tests always decreases. As expected, the drop in surface area is more prominent as the temperature

rises, reaching the minimum value of 0.2 m^2/g at 750 °C. Looking at the BET value of the fresh samples, it is evident that Al_2O_3 addition enhances the surface area, from 1.2 m^2/g to 9 m^2/g in the case of 98Fe2Al and 60Fe40Al, respectively.

After the stability tests in the 2 steps CLH, the surface area of the sample 60Fe40Al undergoes an 86.7 % decrease with respect to its original value (from 9 m^2/g to 1.3 m^2/g at 675 °C). The effect of temperature on the decrease of surface area is not substantial, only a slight negative trend is observed going from 1.3 m^2/g at 675 °C to 1.2 m^2/g at 750 °C. However, the drop in BET surface area in the 3 step CLH is only of 33.0 % varying from 9.0 m^2/g to 6.2 m^2/g after the test at 675 °C and it remains almost constant with reaction temperature. This different behavior can be related to the different chemical composition of the sample at the end of the CLH tests in the 2 and 3 steps configuration (Figure 1). In the 2 steps CLH the sample is composed by a mixture of $FeAl_2O_4/Fe_3O_4$ in different proportion according to the reaction temperature. At the end of stability test in the 3 step CLH the $FeAl_2O_4$ is converted into Fe_2O_3 and Al_2O_3 by the addition of the air oxidation step [28]. On the contrary, the BET values of the sample 98Fe2Al at the end of the stability tests are always close to the fresh one (fresh sample 1.2 m^2/g, 1.0 m^2/g at 750 °C).

The TPR profiles of the pure Fe_2O_3 and of samples 60Fe40Al and 98Fe2Al are reported in Figure 2 a-c. The TPR profile of pure Fe_2O_3 (Figure 2a) shows that the reduction to metallic iron occurs into mainly three phases partially overlapped: 1) Fe_2O_3 reduction (red curve) occurs in the temperature range 400-450 °C with the highest weight loos rate at 425 °C; 2) the reduction of Fe_3O_4 to FeO (light-blue curve) starts at 400 °C with a maximum weight loss rate at 500 °C and the complete reduction to FeO is reached at 600 °C; 3) FeO reduction to metallic Fe (green curve) occurs in the temperature range (500-600 °C) having the maximum weight loss rate at 550 °C. The complete reduction to Fe is reached at 600 °C.

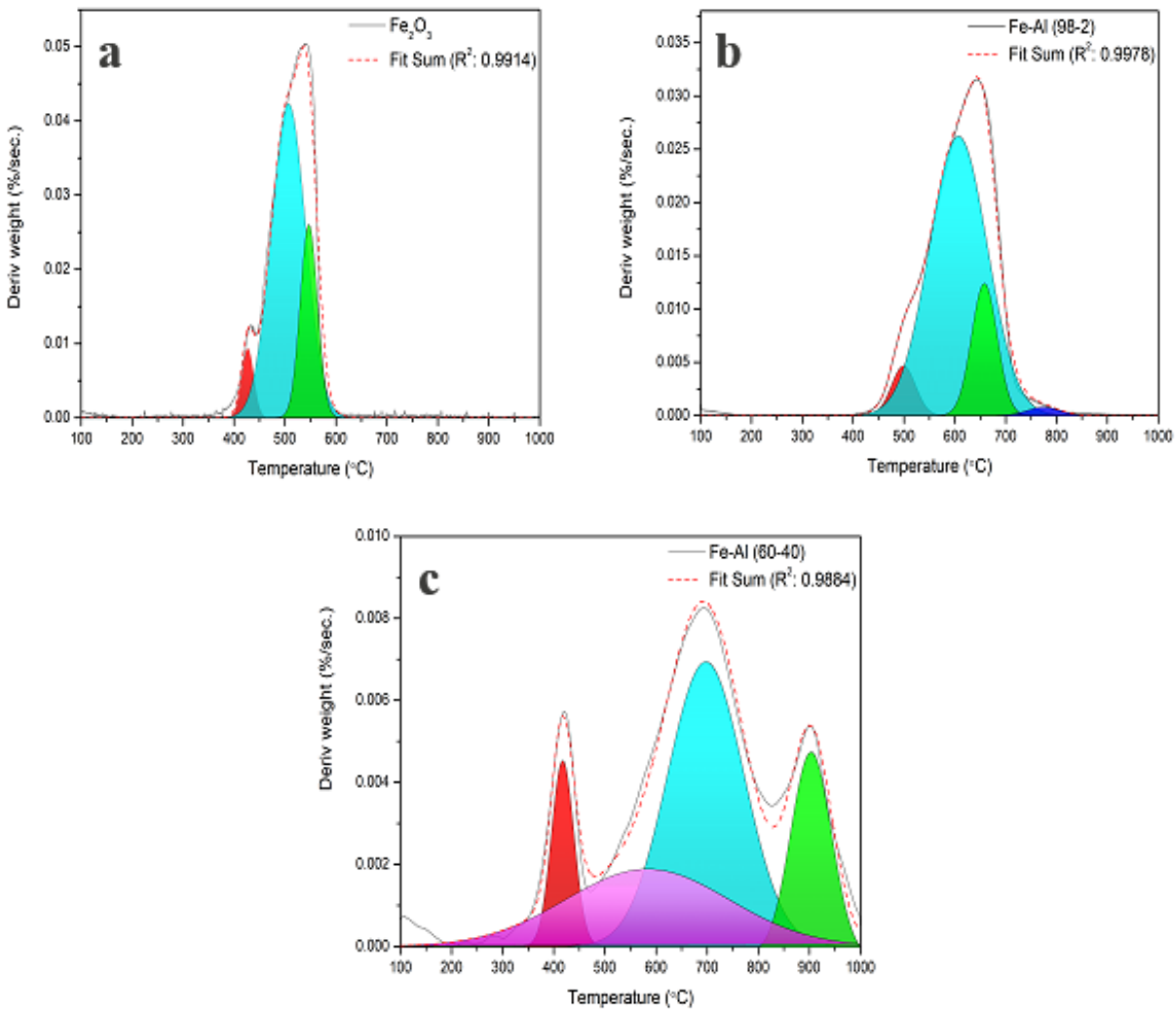

Figure 2. TPR profiles of (a) pure Fe_2O_3, (b) 98Fe2Al, and (c) 60Fe40Al. Red: reduction of Fe_2O_3 to Fe_3O_4; light-blue: reduction of Fe_3O_4 to FeO; green: reduction of FeO to Fe; blue: conversion of $FeAl_2O_4$ into Fe and Al_2O_3.

When Al_2O_3 was added to hematite, the rate of iron oxides reduction completely changes. Specifically, a lag effect on the iron oxide reduction rate is registered. Observing the TPR profile of the sample 98Fe2Al (Figure 2b), the effect of the chemical reaction between FeO and Al_2O_3 to produce $FeAl_2O_4$ is clearly visible. The peak at 500 ºC corresponds to the hematite reduction to magnetite which is increased by 50 ºC compared to the results of pure Fe_2O_3 sample. In the

reduction region from Fe_3O_4 to FeO (light-blue peak) significant differences are detected: in sample 98Fe2Al the weight loss rate is extended up to 800 °C while with pure Fe_2O_3 the complete reduction of wüstite is already reached to 600 °C. This delay effect introduced by the presence of 2 wt% of Al_2O_3 could be attributed to the formation of the spinel, which increases the complexity of the iron oxides reduction mechanism by adding another reaction in the region of FeO formation, thus causing the enlargement of the peak. It is worth to highlight that the completion of this step of reduction is fundamental to produce hydrogen by chemical looping technology since without the formation of FeO and Fe phase, H_2 cannot be produced by steam oxidation. However, when the amount of Al_2O_3 added to the iron oxides is only 2 wt% of the sample mass, this phenomenon regards only a small fraction of the wüstite produced and the free FeO can be rapidly reduced to iron highlighted by the green peak at 650 °C. For the conversion of $FeAl_2O_4$ into Fe and Al_2O_3, higher temperature is needed (790 °C, blue peak).

The TPR profiles of the sample 60Fe40Al (Figure 2c), highlight the negative effect of $FeAl_2O_4$ formation on iron oxides reduction rate. For the sample 60Fe40Al the complete reduction to metallic iron is achieved at temperatures significantly higher than those required for pure Fe_2O_3; the reduction to Fe can be considered complete only at 1000 °C. The violet peaks detected over the whole temperature range examined, can be related to the diffusion limitations introduced in the solid matrix by the formation of the spinel ($FeAl_2O_4$), which makes it difficult to desorb water produced by reduction with hydrogen. The phenomenon became more visible with the sample 60Fe40Al as it owns an increased specific surface area and therefore a better accessibility of iron active sites.

Influence of temperature on ethanol cracking products. At temperature higher than 500 °C ethanol starts to decompose producing mainly H_2, CO and solid carbon. In an authors' previous

work, the thermal ethanol decomposition pathway was studied at 675 °C and atmospheric pressure [22]. Based on the results, ethanol can be completely decomposed into a gaseous mixture mainly constituted by syngas and methane, which undergoes cracking reaction becoming responsible for coke formation.

To evaluate the influence of temperature on the ethanol decomposition pathway, blank tests were performed by feeding ethanol on an inert solid bed (SiO_2) at the two different reaction temperatures (675 °C and 750 °C) studied. Table 3 reports the molar fraction of the products obtained (carrier free basis).

Table 3. Thermal ethanol decomposition products and carrier free molar fraction at 675 °C and 750°C.

Temperature (°C)	H_2 (%)	CO (%)	CH_4 (%)	Carbon (%)
675	58.0	18.0	7.0	17.0
750	60.5	17.2	3.2	19.1

Looking at Table 3, the variation of temperature in the range 675-750 °C affects the molar fraction of the products. At 750 °C, the H_2 and C molar fractions increase of approximately 5 % and 12 %, respectively, compared to the value at 675 °C, while methane decreases of 55 %. Otherwise, no significant variation of CO concentration with temperature was detected.

These results suggest that the increase of temperature in the range examined, enhances the methane cracking favoring the ethanol conversion into H_2 and C, obtaining a higher reduction force stream. Based on thermodynamic evaluations, the higher concentration of reductants allows to achieve a deeper reduction of iron oxides without increase the temperature [42]. However, the iron oxides reduction reactions by carbon still owns slow kinetics over the range of temperatures studied (675-750 °C) [43,44] and if it is not consumed by reduction reactions it could be gasified during the oxidation step (reaction 2) producing CO together with hydrogen.

$$C + H_2O \leftrightarrow CO + H_2 \qquad (2)$$

Aiming at the production of H_2 free of CO, the amount of carbon deposited on the surface of the reduced iron particles is a key parameter, which must be carefully controlled.

Determination of the optimal amount of ethanol fed for pure H_2 production: 1 redox cycles at 675 °C and 750 °C. The control of iron oxides reduction degree is one of the strategies to avoid the carbon deposition during the reduction step. As already explained, in fact, if the reduction of the sample is carried until completion to Fe phase, oxygen is not present anymore in the system and carbon cannot be converted into CO and CO_2. In this work, the control of iron oxides reduction degree is achieved by monitoring the amount of ethanol fed during the reduction step. However, the decrease of ethanol fed led to a lower iron oxides reduction degree and therefore to a lower hydrogen yield.

The optimal ethanol amount is determined with one redox cycle where the H_2 purity is strictly monitored. Different ethanol amount was fed in reduction (3.42 mmol, 4.57 mmol and 5.71 mmol) at constant flow rate of 4 mL/h by changing the feeding time (3 min, 4 min and 5 min). A fresh sample is used for each amount of ethanol tested and the optimal ethanol amount is defined as the value for which no CO is detected in the H_2 stream. To give an indication of the iron oxides reduction degree achieved at each amount of ethanol, the efficiency of the process (E %) was calculated according to equation 3.

$$E\ (\%) = \ (H_2\ experimetal)/(H_2\ theoretical) * 100 \qquad (3)$$

E (%) is the ratio of the amount of H_2 produced during the experimental oxidation step and the maximum amount of H_2 that, theoretically, can be produced by the sample, considering its complete reduction to Fe and then its complete oxidation to Fe_3O_4. An efficiency value of 100 % means that the complete reduction of samples is achieved.

The comparison of the process efficiency (bars) of the samples 100Fe, 60Fe40Al and 98Fe2Al as a function of the amount of ethanol fed (3.42, 4.57 and 5.71 mmol) at 675 °C is reported in Figure 3. The maximum CO concentration measured (if present) is also reported in the graphs (line).

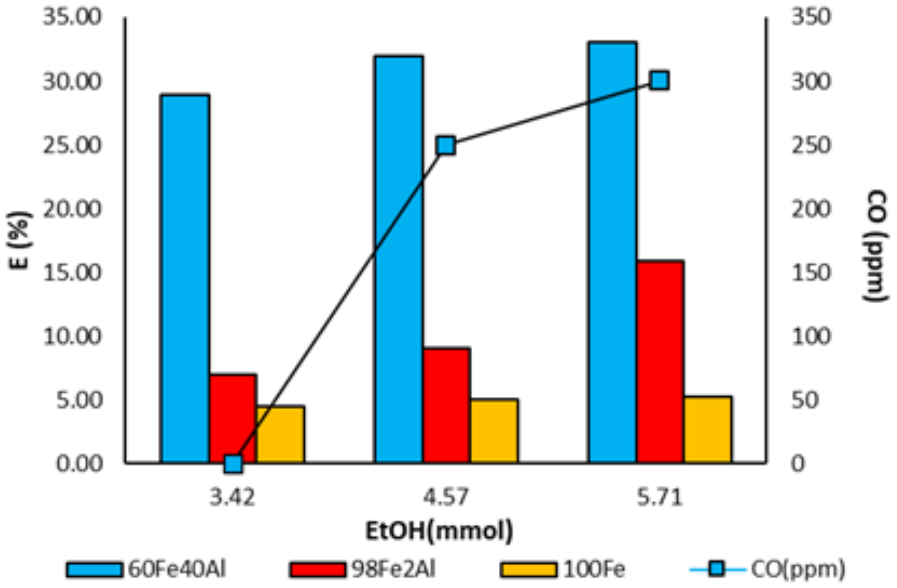

Figure 3. Process efficiency (bars) and CO maximum concentration (lines) obtained with the samples 60Fe40Al, 98Fe2Al and 100Fe at 675 °C.

The results reported in Figure 3 highlight the relationship between amount of ethanol fed and hydrogen yields; at constant reduction temperature, by increasing the amount of ethanol fed a higher process efficiency values were always obtained suggesting that a deeper iron oxides reduction is achieved. The need to control the reduction degree significantly limit the reactivity of the sample 100Fe, which produces H_2 only for the 5.2 % of its total amount producible (H_2 theoretical). The low reactivity of 100Fe is strongly connected to the morphology of the sample. As described in Table 2, it appears as a non-porous material with a very low specific surface area (0.7 m^2/g), that causes severe diffusion limitations of gaseous reductants in the particle core [45].

The addition of Al_2O_3 to hematite increases the hydrogen yields proportionally to the amount of Al_2O_3 added; the highest process efficiency values of approximately 30 % was obtained with the sample 60Fe40Al in all ethanol range studied while the sample 98Fe2Al produces a maximum efficiency value of 15 % when 5.71 mmol of ethanol were fed. The higher redox activity of 60Fe40Al is linked to the sample morphology modification induced by the addition of high amount of Al_2O_3 (Table 2), which increases the specific surface area of the sample and therefore improves the accessibility of iron active sites. In the case of 98Fe2Al, the low amount of Al_2O_3 added not confers the same improvement (Table 2); the BET value is higher than the sample 100Fe (1.5 m^2/g for 98Fe2Al and 0.7 m^2/g for 100Fe) but it is still low to avoid the severe diffusion limitations of gaseous reductants in the particle core [45].

Looking at the CO profile in the Figure 3 is clear that the amount of Al_2O_3 added to hematite significantly affects the hydrogen purity; with the sample 100Fe and 98Fe2Al a pure H_2 stream is always produced while the sample with higher amount of Al_2O_3 added (40 wt%) pure H_2 is produced only when 3.42 mmol of ethanol are fed. The higher rate of carbon formation registered with the sample 60Fe40Al confirms the catalytic activity of Al_2O_3 in cracking reactions, which became more prominent when a high amount of Al_2O_3 is added to the sample.

The increase of reaction temperature enhances the hydrogen yield promoting both thermodynamics and kinetics of iron oxide reduction [46,47]. However, as demonstrated in the blank tests of ethanol decomposition (Table 3), temperature also increases the rate of solid carbon formation. Figure 4 reports the process efficiency and CO profile registered with the samples 60Fe40Al, 98Fe2Al and 100Fe when the reaction temperature is 750 °C.

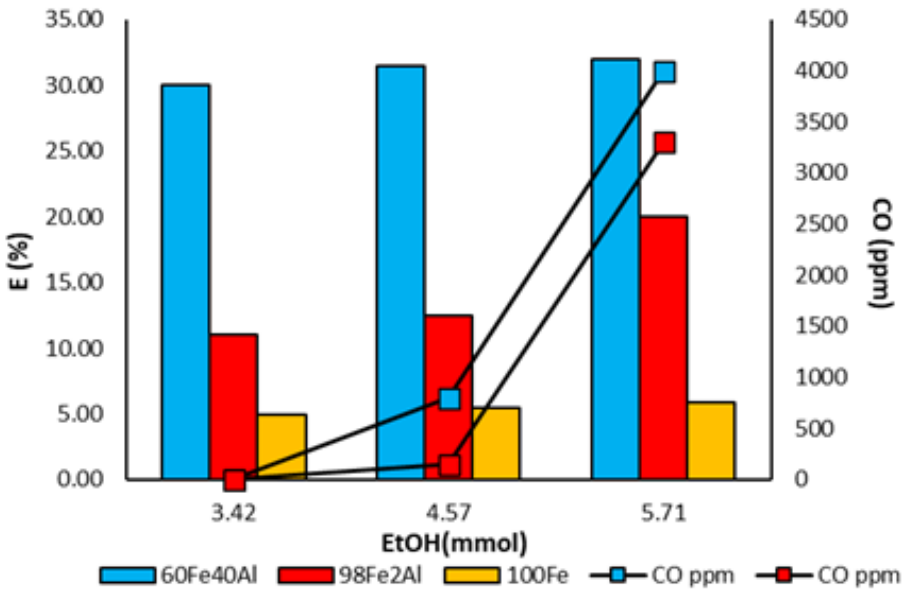

Figure 4. Process efficiency values (bars) and CO profile (lines) obtained with the sample 100Fe, 60Fe40Al and 98Fe2Al at 750 °C.

The temperature variation acts differently for the two samples with Al_2O_3 in terms of process efficiency value. In the case of 60Fe40Al the temperature does not have significant influence on the efficiency, which at 750 °C is only 6 % higher than the value at 675 °C. On the contrary, for the sample 98Fe2Al the increase of temperature led to an enhancement of the particle activity; the efficiency value changes from 5.2 % at 675 °C to 12 % at 750 °C at constant ethanol fed of 3.42 mmol. This behavior is strongly connected to the different morphology of the samples and therefore to the accessibility of the Fe active sites, which in the case of 60Fe40Al are already accessible at the lower temperatures. When the amount of Al is reduced (98Fe2Al) the rise of the temperature favors the diffusion and kinetic enhancing the sample reduction [47].

The negative effect of the presence of Al_2O_3 on the H_2 purity became more visible in the redox test at 750 °C; the sample 100Fe still produce pure H_2 in all ethanol range while both samples with Al_2O_3 were able to produce it only when 3.42 mmol of ethanol were fed. These results confirm the difficulty to fully exploit the reducing power of carbon to convert iron oxides to iron when the

reaction temperature is in the range 675-750 °C. It is, indeed, well known from literature that the use of carbon as reductant needs temperatures higher than 900 °C [48,49].

Influence of temperature on sample stability: Fe/Al interaction into 2 steps CLH. To evaluate the resistance at high temperature and the particles reactivity at repeated cycles, stability tests consisting into 10 consecutive redox cycles are performed. All the experiments are conducted feeding 3.42 mmol of ethanol in reduction, amount for which pure hydrogen is obtained at each temperature with all samples. The influence of increasing reaction temperature on both efficiency and particles long-term activity is investigated.

Figure 5 reports a comparison of the process efficiency (E %) for 10 consecutive cycles of the three samples (100Fe, 60Fe40Al and 98Fe2Al) as a function of the reaction temperature.

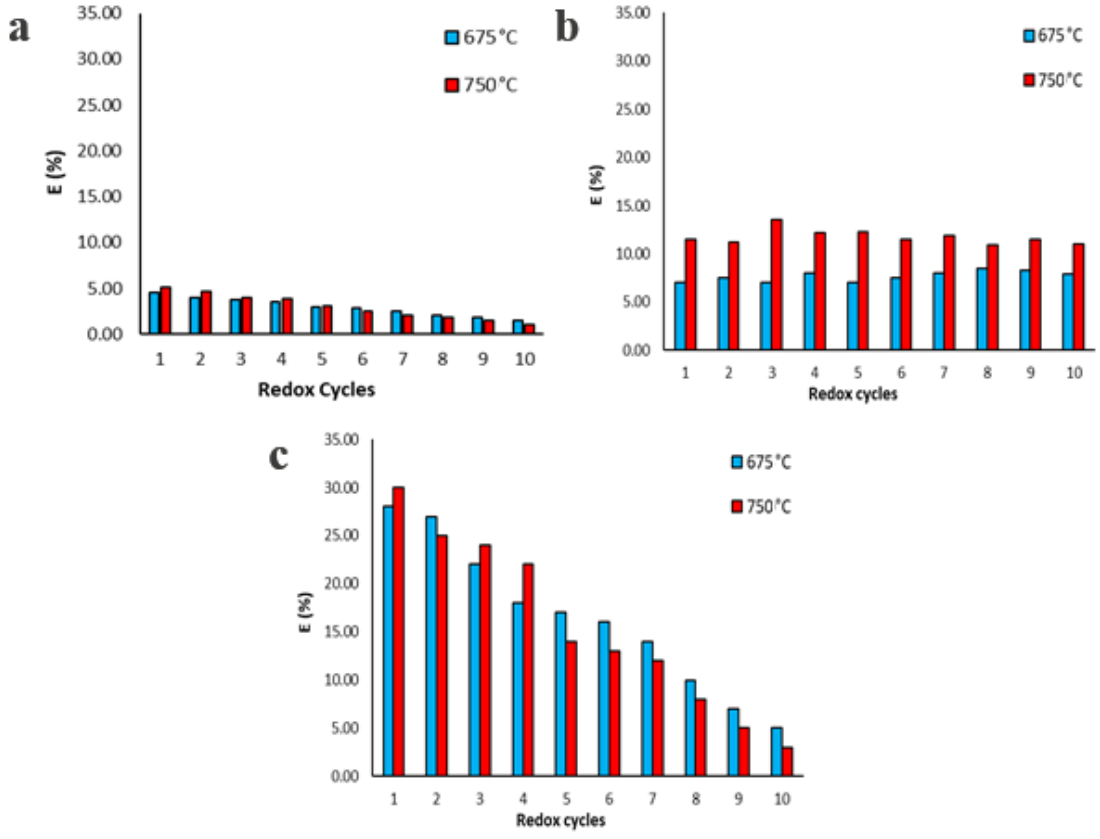

Figure 5. Process efficiency values for 10 consecutive redox cycles when 3.42 mmol of EtOH are fed in 2 steps CLH. (a) 100Fe, (b) 98Fe2Al, and (c) 60Fe40Al.

The results obtained with the sample 100Fe (Figure 5a) highlight the two main issues related to the utilization of pure Fe in the process: the low accessibility of the active sites and the poor thermal stability. The low accessibility of the active sites is responsible for the low value of the process efficiency (highest value equal to 6.1 %) while the poor thermal stability is visible from the sample deactivation at repeated cycles. In addition, the positive effect induced by the higher temperatures on the reduction capability and consequently on H_2 yields is not maintained for all the cycles. In fact, starting from the cycle number 5, a sharp decrease of process efficiency at the highest tested temperature (750 °C) is registered; the H_2 yields decrease continuously till the 10^{th} cycle in which the minimum efficiency value is reached (E =1.52 %). The results confirm the impossibility of using pure Fe in the proposed system due to the very low thermal stability which, as expected, worsen as the temperature increases [50].

Looking at the results reported in Figure 5, the added amount of Al_2O_3 is demonstrated to be a key parameter also on the long-term particle performances. At the higher Al_2O_3 content (60Fe40Al), the sample shows a sharp decrease of the efficiency whereas the 98Fe2Al maintains constant its activity, with a slight variation of 10 % around a medium efficiency value.

The efficiency of the sample 60Fe40Al (Figure 5c) assumes the highest values among all the tested samples in the first few cycles, but a rapid deactivation is registered at each tested temperature. The increase of temperature has opposite effects in the process: it increases the hydrogen yield but enhancing the spinel formation ($FeAl_2O_4$) lead to sample deactivation. In fact, the enhanced temperature improves the efficiency only till the 4^{th} cycle, while starting from cycles number 5 the trend becomes opposite (Figure 5c) and the efficiency values at higher temperature becomes lower those at 675 °C. These results demonstrate that the deactivation rate of 60Fe40Al depends on the reaction temperature, becoming faster at high temperature due to the formation of

$FeAl_2O_4$, as detected by XRD analyses (Figure 1). Several works in literature studied the $FeAl_2O_4$ formation in chemical looping H_2 processes [29,51,52] but the kinetics and reaction mechanism of hercynite redox cycles are still poorly understood.

The proposed redox mechanism of Fe/Al particles is reported in reactions 4-10

Reduction pathway with H_2 of Fe/Al particles

$$3Fe_2O_3 + Al_2O_3 + H_2 \leftrightarrow 2Fe_3O_4 + Al_2O_3 + H_2O \quad (4)$$

$$Fe_3O_4 + Al_2O_3 + H_2 \leftrightarrow 3FeO + Al_2O_3 + H_2O \quad (5)$$

$$FeO + Al_2O_3 \leftrightarrow FeAl_2O_4 \quad (6)$$

$$FeAl_2O_4 + H_2 \leftrightarrow Fe + Al_2O_3 + H_2O \quad (7)$$

Steam Oxidation pathway

$$Fe + Al_2O_3 + H_2O \leftrightarrow FeO + Al_2O_3 + H_2 \quad (8)$$

$$FeO + Al_2O_3 \leftrightarrow FeAl_2O_4 \quad (9)$$

Air Oxidation

$$2FeAl_2O_4 + 0.5\ O_2 \leftrightarrow Fe_2O_3 + 2Al_2O_3 \quad (10)$$

$FeAl_2O_4$ results from the interaction of wüstite (FeO) with Al_2O_3 and, according to the redox iron pathway, the FeO can be formed in both the process steps after the reduction from Fe_3O_4 and after the iron oxidation with steam [53]. Furthermore, the $FeAl_2O_4$ oxidation with steam is not thermodynamically favored [54] and therefore when the formation of the spinel occurs, the steam oxidation is not able to recover the two separated oxides, which can be restored only using a more sever oxidation step with air (reaction 10) or by a deeper reduction (reaction 7) [55]. However, this last option would require larger amount of ethanol in reduction, which are not compatible with the production of pure H_2 as demonstrated by the performed tests.

For the sample 60Fe40Al, the kinetic of formation of $FeAl_2O_4$ makes the reduction step slower. Furthermore, the $FeAl_2O_4$ formation is favored at higher temperature, in fact, the sample at the end of the stability test performed at 750 °C is composed entirely by $FeAl_2O_4$ (Figure 1) [11]. Based on the results obtained by the stability tests, it seems that the formation of the spinel takes place very slowly with the increase of the cycle numbers. The slow increase of the spinel phase makes the sample 60Fe40Al more and more inert in the process, leading to its deactivation.

The different behavior of 98Fe2Al sample in terms of particle stability is explained by the lower amount of Al_2O_3 added in the sample and, thus, on the Fe/Al interaction in the formation of the spinel. In fact, the formation of the spinel subtracts to the active sites only a small fraction of Fe, therefore the sample is active and stable for 10 consecutive redox cycles. This result suggests that the spinel owns the same properties of Al_2O_3 giving to the sample high thermal resistance.

3 steps CLH configuration: influence of adding an air oxidation step on the reactivity of the sample 60Fe40Al. To make possible the utilization of high Al_2O_3 concentration as iron oxides structural promoter, in order of fully exploit the high activity of this material, the sample 60Fe40Al is tested in the 3 steps CLH process. The 3 step CLH consists in a reduction, in a steam oxidation and in an air oxidation step. The air oxidation step makes possible the $FeAl_2O_4$ oxidation into Fe_2O_3 and Al_2O_3 restoring the sample activity (reaction 10) [56].

The 3 steps CLH configuration is tested only with the sample 60Fe40Al, which showed strong deactivation in the 2 steps configuration. Figure 6 reports the efficiency of the process for 10 redox cycles as function of temperature. The results confirm that the presence of the air oxidation let to overcome the issue of the interaction of Fe/Al in the 2 steps CLH at the expense of the complexity of the system, which requires an additional unit for the air oxidation step. By increasing the temperature, the H_2 yields are always higher without registering any deactivation.

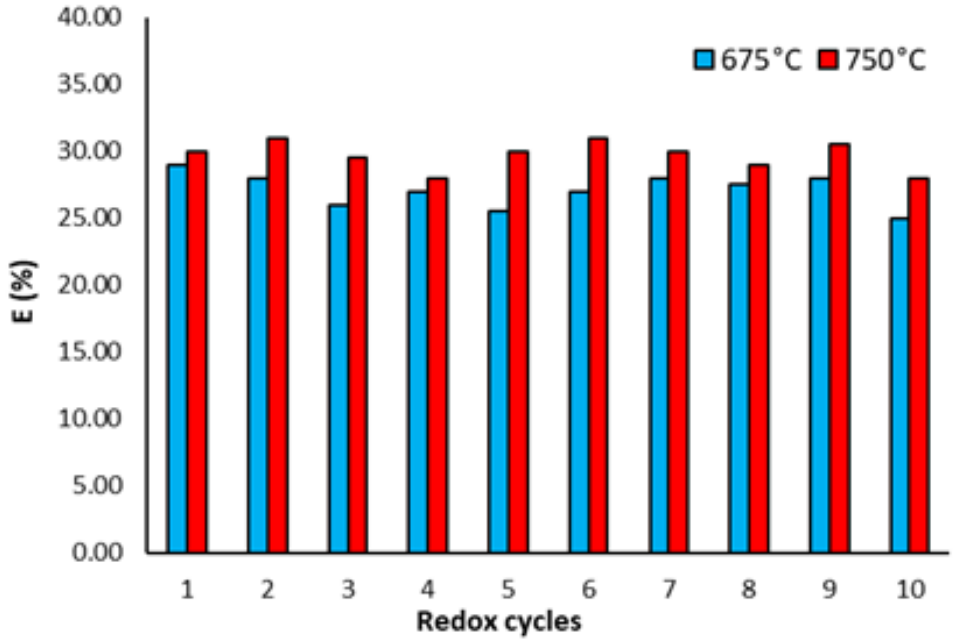

Figure 6. Process efficiency of the sample 60Fe40Al as a function of temperature in the 3 steps CLH configuration.

CONCLUSIONS

A stable production of pure H_2 by Chemical Looping Hydrogen process (CLH) process was demonstrated to be feasible using bioethanol as renewable reductant and Fe/Al_2O_3 as redox system. The role of Al_2O_3 was studied by adding two different amounts of Al_2O_3 to iron oxides (2 wt% and 40 wt%). The Fe/Al interactions were evaluated in a fixed bed reactor working in two different configurations: 2 and 3 steps CLH.

To avoid the carbon deposition during the reduction step, the iron oxides reduction degree is controlled at each tested temperature (675-750 °C) by monitoring the amount of ethanol fed. The results demonstrated that the carbon deposition rate depends on temperature and Al_2O_3 concentration in the sample mass and that, to preserve hydrogen purity, the oxides cannot be fully reduced, lowering the process efficiency.

When high amount of Al_2O_3 is used, the formation of the spinel $FeAl_2O_4$ takes place, hindering the activity of the material due to its behavior as inert material in the 2 step CLH. The spinel formation is significantly affected by the reaction temperature, becoming faster at 750 °C and so leading to a faster sample deactivation. By decreasing the amount of Al_2O_3 added to 2 wt%, and so limiting the spinel formation, the iron thermal stability is improved. Indeed, the sample produces stable H_2 yield for 10 cycles with a positive effect on the iron reducibility, especially at 750 °C.

To maintain high H_2 yields using 60Fe40Al, the addition of a further oxidation step with air (3 steps CLH) was found to be fundamental to restore the Fe redox activity, converting the inert $FeAl_2O_4$ into the two separated oxides (Fe_2O_3 and Al_2O_3). In this way the successful utilization of this material with a constant process efficiency for 10 cycles is obtained, demonstrating the feasibility of the process with an efficiency of about 30 % at 750 °C.

AUTHOR INFORMATION

Corresponding Author

Maria P. Bracciale- Department of Chemical Engineering Materials Environment, SAPIENZA University of Rome, Via Eudossiana 18, 00184, Rome (Italy);

e-mail: mariapaola.bracciale@uniroma1.it

Authors

Martina Damizia- Department of Chemical Engineering Materials Environment, SAPIENZA University of Rome, Via Eudossiana 18, 00184, Rome (Italy), martina.damizia@uniroma1.it;

Francesco Anania- Department of Chemical Engineering Materials Environment, SAPIENZA University of Rome, Via Eudossiana 18, 00184, Rome (Italy), francesco.anania@uniroma1.it;

Lingyu Tai- Key Laboratory of Agro-Forestry Environmental Processes and Ecological Regulation of Hainan Province-College of Ecology & Environment, Hainan University, 570228, Haikou (China), tailingyutju@163.com;

Paolo De Filippis- Department of Chemical Engineering Materials Environment, SAPIENZA University of Rome, Via Eudossiana 18, 00184, Rome (Italy), paolo.defilippis@uniroma1.it;

Benedetta de Caprariis- Department of Chemical Engineering Materials Environment, SAPIENZA University of Rome, Via Eudossiana 18, 00184, Rome (Italy), benedetta.decaprariis@uniroma1.it;

Author Contributions

The manuscript was written through contributions of all authors. All authors have given approval to the final version of the manuscript.

Notes

The authors declare no competing financial interest.

REFERENCES

[1] Xie F, Shao Z, Hou M, Yu H, Song W, Sun S, et al. Recent progresses in H2-PEMFC at DICP. Journal of Energy Chemistry 2019;36:129–40. https://doi.org/10.1016/J.JECHEM.2019.07.012.

[2] Ramli ZAC, Kamarudin SK. Platinum-Based Catalysts on Various Carbon Supports and Conducting Polymers for Direct Methanol Fuel Cell Applications: a Review. Nanoscale Research Letters 2018 13:1 2018;13:1–25. https://doi.org/10.1186/S11671-018-2799-4.

[3] Dincer I. Green methods for hydrogen production. International Journal of Hydrogen Energy 2012;37:1954–71. https://doi.org/10.1016/J.IJHYDENE.2011.03.173.

[4] Muradov N. Low to near-zero CO2 production of hydrogen from fossil fuels: Status and perspectives. International Journal of Hydrogen Energy 2017;42:14058–88. https://doi.org/10.1016/J.IJHYDENE.2017.04.101.

[5] Howarth RW, Jacobson MZ. How green is blue hydrogen? Energy Science & Engineering 2021;9:1676–87. https://doi.org/10.1002/ESE3.956.

[6] Holladay JD, Hu J, King DL, Wang Y. An overview of hydrogen production technologies. Catalysis Today 2009;139:244–60. https://doi.org/10.1016/J.CATTOD.2008.08.039.

[7] Tozer L, Klenk N. Discourses of carbon neutrality and imaginaries of urban futures. Energy Research & Social Science 2018;35:174–81. https://doi.org/10.1016/J.ERSS.2017.10.017.

[8] Luo M, Yi Y, Wang S, Wang Z, Du M, Pan J, et al. Review of hydrogen production using chemical-looping technology. Renewable and Sustainable Energy Reviews 2018;81:3186–214. https://doi.org/10.1016/J.RSER.2017.07.007.

[9] Tong A, Bayham S, Kathe M V., Zeng L, Luo S, Fan LS. Iron-based syngas chemical looping process and coal-direct chemical looping process development at Ohio State University. Applied Energy 2014;113:1836–45. https://doi.org/10.1016/J.APENERGY.2013.05.024.

[10] Hoxha A, Palone O, Cedola L, Stendardo S, Borello D. Development of a novel carbon capture and utilization approach for syngas production based on a chemical looping cycle. Fuel 2022;325:124760. https://doi.org/10.1016/J.FUEL.2022.124760.

[11] Voitic G, Hacker V. Recent advancements in chemical looping water splitting for the production of hydrogen. RSC Advances 2016;6:98267–96. https://doi.org/10.1039/C6RA21180A.

[12] Moghtaderi B. Review of the Recent Chemical Looping Process Developments for Novel Energy and Fuel Applications. Energy Fuels 2012;26:15–40. https://doi.org/10.1021/ef201303d.

[13] Yuan J, Wang W, Zhu S, Wang F. Comparison between the oxidation of iron in oxygen and in steam at 650–750 °C. Corrosion Science 2013;75:309–17. https://doi.org/10.1016/J.CORSCI.2013.06.014.

[14] Rydén M, Arjmand M. Continuous hydrogen production via the steam–iron reaction by chemical looping in a circulating fluidized-bed reactor. International Journal of Hydrogen Energy 2012;37:4843–54. https://doi.org/10.1016/J.IJHYDENE.2011.12.037.

[15] Chiesa P, Lozza G, Malandrino A, Romano M, Piccolo V. Three-reactors chemical looping process for hydrogen production. International Journal of Hydrogen Energy 2008;33:2233–45. https://doi.org/10.1016/J.IJHYDENE.2008.02.032.

[16] Xu T, Xiao B, Fu G, Yang S, Wang X. Chemical looping hydrogen production with modified iron ore as oxygen carriers using biomass pyrolysis gas as fuel 2019. https://doi.org/10.1039/c9ra08936e.

[17] Situmorang YA, Zhao Z, An P, Yu T, Rizkiana J, Abudula A, et al. A novel system of biomass-based hydrogen production by combining steam bio-oil reforming and chemical looping process. Applied Energy 2020;268:115122. https://doi.org/10.1016/J.APENERGY.2020.115122.

[18] Kong F, Swift J, Zhang Q, Fan LS, Tong A. Biogas to H2 conversion with CO2 capture using chemical looping technology: Process simulation and comparison to conventional reforming processes. Fuel 2020;279:118479. https://doi.org/10.1016/J.FUEL.2020.118479.

[19] Gremyachkin VM, Mazanchenko EP. Gasification of porous carbon particle by steam. Russian Journal of Physical Chemistry B 2009 3:4 2009;3:595–601. https://doi.org/10.1134/S1990793109040125.

[20] Zhu M, Chen S, Soomro A, Hu J, Sun Z, Ma S, et al. Effects of supports on reduction activity and carbon deposition of iron oxide for methane chemical looping hydrogen generation. Applied Energy 2018;225:912–21. https://doi.org/10.1016/J.APENERGY.2018.05.082.

[21] Ma S, Chen S, Soomro A, Xiang W. Effects of supports on hydrogen production and carbon deposition of Fe-based oxygen carriers in chemical looping hydrogen generation. International Journal of Hydrogen Energy 2017;42:11006–16. https://doi.org/10.1016/J.IJHYDENE.2017.02.132.

[22] De Filippis P, D'Alvia L, Damizia M, de Caprariis B, Del Prete Z. Pure hydrogen production by steam-iron process: The synergic effect of MnO2 and Fe2O3. International Journal of Energy Research 2020. https://doi.org/10.1002/er.6117.

[23] Bracciale MP, Damizia M, De Filippis P, de Caprariis B. Clean Syngas and Hydrogen Co-Production by Gasification and Chemical Looping Hydrogen Process Using MgO-Doped Fe2O3 as Redox Material. Catalysts 2022;12. https://doi.org/10.3390/CATAL12101273.

[24] Bohn CD, Cleeton JP, Müller CR, Chuang SY, Scott SA, Dennis JS. Stabilizing iron oxide used in cycles of reduction and oxidation for hydrogen production. Energy and Fuels 2010;24:4025–33. https://doi.org/10.1021/ef100199f.

[25] Ma S, Chen S, Soomro A, Xiang W. Effects of CeO2, ZrO2, and Al2O3 Supports on Iron Oxygen Carrier for Chemical Looping Hydrogen Generation. Energy and Fuels 2017;31:8001–13. https://doi.org/10.1021/ACS.ENERGYFUELS.7B01141.

[26] Tijani MM, Aqsha A, Mahinpey N. Synthesis and study of metal-based oxygen carriers (Cu, Co, Fe, Ni) and their interaction with supported metal oxides (Al2O3, CeO2, TiO2, ZrO2) in a chemical looping combustion system. Energy 2017;138:873–82. https://doi.org/10.1016/J.ENERGY.2017.07.100.

[27] Marturano M, Aglietti EF, Ferretti O. α-Al2O3 Catalyst supports for synthesis gas production: influence of different alumina bonding agents on support and catalyst properties. Materials Chemistry and Physics 1997;47:252–6. https://doi.org/10.1016/S0254-0584(97)80060-0.

[28] Liu W, Ismail M, Dunstan MT, Hu W, Zhang Z, Fennell PS, et al. Inhibiting the interaction between FeO and Al 2 O 3 during chemical looping production of hydrogen 2015. https://doi.org/10.1039/c4ra11891j.

[29] Sarkar R, Sohn HY. Interaction of ferrous oxide with alumina refractory under flash ironmaking conditions. Ceramics International 2019;45:15417–28. https://doi.org/10.1016/J.CERAMINT.2019.05.040.

[30] Liu W, Ismail M, Dunstan MT, Hu W, Zhang Z, Fennell PS, et al. Inhibiting the interaction between FeO and Al2O3 during chemical looping production of hydrogen. RSC Advances 2014;5:1759–71. https://doi.org/10.1039/C4RA11891J.

[31] Wang Q, Li W, Hung I, Mentink-Vigier F, Wang X, Qi G, et al. Mapping the oxygen structure of γ-Al2O3 by high-field solid-state NMR spectroscopy. Nature Communications 2020 11:1 2020;11:1–9. https://doi.org/10.1038/s41467-020-17470-4.

[32] Keller M, Matsumura A, Sharma A. Spray-dried Fe/Al2O3 as a carbon carrier for COx-free hydrogen production via methane cracking in a fluidized bed process. Chemical Engineering Journal 2020;398:125612. https://doi.org/10.1016/J.CEJ.2020.125612.

[33] Wang W, Fan L, Wang G. Study on chemical looping reforming of ethanol (CLRE) for hydrogen production using NiMn2O4 spinel as oxygen carrier. Journal of the Energy Institute 2017;90:884–92. https://doi.org/10.1016/J.JOEI.2016.08.006.

[34] Li L, Jiang B, Tang D, Zheng Z, Zhao C. Hydrogen Production from Chemical Looping Reforming of Ethanol Using Ni/CeO2 Nanorod Oxygen Carrier. Catalysts 2018, Vol 8, Page 257 2018;8:257. https://doi.org/10.3390/CATAL8070257.

[35] García-Labiano F, García-Díez E, De Diego LF, Serrano A, Abad A, Gayán P, et al. Syngas/H2 production from bioethanol in a continuous chemical-looping reforming prototype. Fuel Processing Technology 2015;137:24–30. https://doi.org/10.1016/J.FUPROC.2015.03.022.

[36] Vozniuk O, Cacciaguerra T, Tanchoux N, Albonetti S, Stievano L, Millet J-MM, et al. Control of the mechanism of chemical-looping of ethanol in non-stoichiometric ferrites by Cu-Mn substitution. Catal Today 2023:114105. https://doi.org/10.1016/J.CATTOD.2023.114105.

[37] Trevisanut C, Mari M, Millet JM, Cavani F. Chemical-loop reforming of ethanol over metal ferrites: An analysis of structural features affecting reactivity. Int J Hydrogen Energy 2015;40:5264–71. https://doi.org/10.1016/J.IJHYDENE.2015.01.054.

[38] de Caprariis B, Damizia M, De Filippis P, Bracciale MP. The role of Al2O3, MgO and CeO2 addition on steam iron process stability to produce pure and renewable hydrogen. International Journal of Hydrogen Energy 2021;46:39067–78. https://doi.org/10.1016/J.IJHYDENE.2021.09.135.

[39] Graulis S, Chateigner D, Downs RT, Yokochi AFT, Quirós M, Lutterotti L, et al. Crystallography Open Database - An open-access collection of crystal structures. J Appl Crystallogr 2009;42:726–9. https://doi.org/10.1107/S0021889809016690.

[40] Kidambi PR, Cleeton JPE, Scott SA, Dennis JS, Bohn CD. Interaction of Iron Oxide with Alumina in a Composite Oxygen Carrier during the Production of Hydrogen by Chemical Looping. Energy Fuels 2012;26:603–17. https://doi.org/10.1021/ef200859d.

[41] Elrefaie FA, Smeltzer WW. Thermodynamics of the system iron-aluminum-oxygen between 1073 K and 1573 K. Metallurgical Transactions B 1983 14:1 1983;14:85–93. https://doi.org/10.1007/BF02654055.

[42] Yucel O, Demirci F, Turan A, Alkan M. Determination of direct reduction conditions of mill scale. High Temperature Materials and Processes 2013;32:405–12. https://doi.org/10.1515/HTMP-2012-0167/MACHINEREADABLECITATION/RIS.

[43] Shafiefarhood A, Hamill JC, Neal LM, Li F. Methane partial oxidation using FeOx@La0.8Sr0.2FeO3−δ core–shell catalyst – transient pulse studies. Physical Chemistry Chemical Physics 2015;17:31297–307. https://doi.org/10.1039/C5CP05583K.

[44] de Diego LF, Ortiz M, Adánez J, García-Labiano F, Abad A, Gayán P. Synthesis gas generation by chemical-looping reforming in a batch fluidized bed reactor using Ni-based oxygen carriers. Chemical Engineering Journal 2008;144:289–98. https://doi.org/10.1016/J.CEJ.2008.06.004.

[45] Doğu TI. The Importance of Pore Structure and Diffusion in the Kinetics of Gas-Solid Non-catalytic Reactions: Reaction of Calcined Limestone with SO2. The Chemical Engineering Journal 1981;21:213–22. https://doi.org/10.1016/0300-9467(81)80005-6.

[46] Ponugoti P V., Garg P, Geddam SN, Nag S, Janardhanan VM. Kinetics of iron oxide reduction using CO: Experiments and Modeling. Chemical Engineering Journal 2022;434:134384. https://doi.org/10.1016/J.CEJ.2021.134384.

[47] Monazam ER, Siriwardane R. Hydrogen Production by Steam Oxidation of Reduced CaFe2O4 during Chemical Looping Coal Gasification: Equilibrium and Kinetic Analysis. Energy and Fuels 2018;32:10398–407. https://doi.org/10.1021/ACS.ENERGYFUELS.8B01650/ASSET/IMAGES/LARGE/EF-2018-01650P_0015.JPEG.

[48] Ubando AT, Chen WH, Ong HC. Iron oxide reduction by graphite and torrefied biomass analyzed by TG-FTIR for mitigating CO2 emissions. Energy 2019;180:968–77. https://doi.org/10.1016/J.ENERGY.2019.05.149.

[49] Ubando AT, Chen WH, Show PL, Ong HC. Kinetic and thermodynamic analysis of iron oxide reduction by graphite for CO2 mitigation in chemical-looping combustion. International Journal of Energy Research 2020;44:3865–82. https://doi.org/10.1002/ER.5184.

[50] Galvita V, Hempel T, Lorenz H, Rihko-Struckmann LK, Sundmacher K. Deactivation of modified iron oxide materials in the cyclic water gas shift process for CO-free hydrogen production. Industrial and Engineering Chemistry Research 2008;47:303–10. https://doi.org/10.1021/IE0708879.

[51] Liu W, Ismail M, Dunstan MT, Hu W, Zhang Z, Fennell PS, et al. Inhibiting the interaction between FeO and Al2O3 during chemical looping production of hydrogen. RSC Advances 2014;5:1759–71. https://doi.org/10.1039/C4RA11891J.

[52] Al-Shankiti IA, Bayon A, Weimer AW. Reduction kinetics of hercynite redox materials for solar thermochemical water splitting. Chemical Engineering Journal 2020;389:124429. https://doi.org/10.1016/J.CEJ.2020.124429.

[53] Bachirou GL, Shuai Y, Zhang J, Huang X, Yuan Y, Tan H. Syngas production by simultaneous splitting of H2O and CO2 via iron oxide (Fe3O4) redox reactions under high-pressure. International Journal of Hydrogen Energy 2016;41:19936–46. https://doi.org/10.1016/J.IJHYDENE.2016.09.053.

[54] Yüzbasi NS, Armutlulu A, Huthwelker T, Abdala PM, Müller CR. Na-β-Al2O3 stabilized Fe2O3 oxygen carriers for chemical looping water splitting: correlating structure with redox stability. Journal of Materials Chemistry A 2022;10:10692–700. https://doi.org/10.1039/D1TA10507H.

[55] Chiu P-C, Ku Y, Wu Y-L, Wu H-C, Kuo Y-L, Tseng Y-H. Characterization and Evaluation of Prepared Fe 2 O 3 /Al 2 O 3 Oxygen Carriers for Chemical Looping Process. Aerosol and Air Quality Research 2014;14:981–90. https://doi.org/10.4209/aaqr.2013.04.0135.

[56] Yüzbasi NS, Kierzkowska A, Müller C. Development of Fe2O3-based, Al2O3-stabilized Oxygen Carriers using Sol-gel Technique for H2 Production via Chemical Looping. Energy Procedia 2017;114:436–45. https://doi.org/10.1016/J.EGYPRO.2017.03.1186.